Novel anion conductors – Conductivity, thermodynamic stability and hydration of anion-substituted mayenite-type cage compounds C12A7:X (X=O, OH, Cl, F, CN, S, N)

Journal:	*Physical Chemistry Chemical Physics*
Manuscript ID:	CP-ART-11-2014-005442.R2
Article Type:	Paper
Date Submitted by the Author:	14-Jan-2015
Complete List of Authors:	Eufinger, Jens-Peter; Justus-Liebig University Giessen, Department of Physical-Chemistry Schmidt, Alexander; TU Berlin, Chemie Lerch, Martin; TU Berlin, Institut für Chemie Janek, Juergen; Justus-Liebig-University Giessen, Department of Physical Chemistry

Novel anion conductors – Conductivity, thermodynamic stability and hydration of anion-substituted mayenite-type cage compounds $C_{12}A_7$:X (X=O, OH, Cl, F, CN, S, N)

Jens-Peter Eufinger,[†] Alexander Schmidt,[‡] Martin Lerch,[‡] Jürgen Janek[,†]*

[†]Physikalisch-Chemisches Institut, Justus-Liebig-Universität Gießen, Heinrich-Buff-Ring 58, 35392 Gießen, Germany

[‡]Institut für Chemie, Technische Universität Berlin, Straße des 17. Juni 135, 10623 Berlin, Germany

solid electrolyte, electrochemical sensors, storage catalysis, cage compound, solid anion conductor, proton conduction

Mayenite ($Ca_{12}Al_{14}O_{33}$) is an highly interesting functional material not only in view of its unique crystal structure as a cage compound but also for its variety of possible applications. Its ability to incorporate foreign ions into the cage structure opens the possibility to create new kinds of solid electrolytes and even of electrides. Therefore, the conductivity of various anion substituted mayenites was measured as a function of temperature. Due to controversial reports on the

stability of mayenite under specific thermodynamic conditions (dry, wet, reducing, high temperature) a comprehensive study on the stability was performed. Mayenite is clearly not stable under dry conditions (ppm H_2O < 100) at temperatures above 1050 °C, and thus, the mayenite phase vanishes from the calcium aluminate phase diagram below a minimum humidity. Two decomposition reactions were observed and are described in detail. To get further insight into the mechanism of hydration of mayenite the conductivity was measured as a function of water vapour pressure in a range of $-5 \leq \lg[p\mathrm{H_2O}/\mathrm{bar}] \leq -1.6$ at temperatures of $1000\ ^\circ\mathrm{C} \leq \theta \leq 1200\ ^\circ\mathrm{C}$. The hydration isotherms are described with high accuracy by the underlying point defect model which is confirmed in a wide range of water vapour pressure.

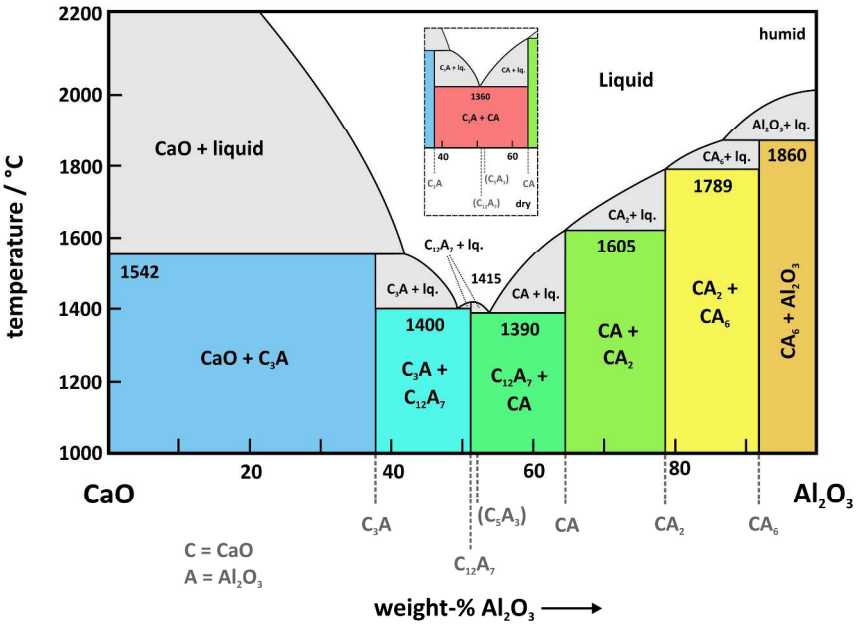

1. Introduction

In the last ten years mayenite ($Ca_{12}Al_{14}O_{33}$, often also denoted as $C_{12}A_7$) attracted serious attention in materials science for its variety of potential applications and for its composition out of ubiquitous elements. In fact, as $Ca_{12}Al_{14}O_{33}$ is a typical phase present in cement, it was quite early well known in concrete research – long before its potential as electrical functional material was recognized.[1-3] In 1988 Irvine *et al.* were the first to report that mayenite is a surprisingly good oxygen ion conductor,[4, 5] with a high oxygen ion mobility being directly related to its unique crystal structure. $C_{12}A_7$ is built up by a three-dimensional network of corner-sharing AlO_4 tetrahedra where the Ca ions are 7-fold coordinated (**Figure 1**). Per formula unit of $Ca_{12}Al_{14}O_{33}$ six cages with a diameter of ~0.4 nm are formed within the structure. And for charge neutrality one of those cages contains a doubly charged oxygen ion which is responsible for the high oxygen ion conductivity.

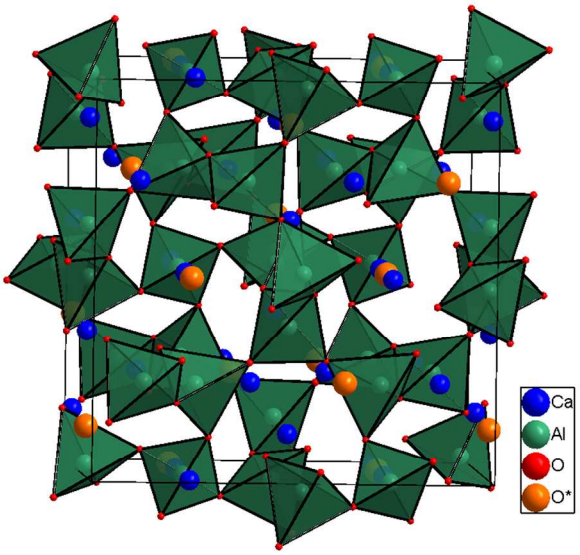

Figure 1. Unit cell of mayenite belonging to space group $I\bar{4}3d$ with Z = 2 (i.e. $Ca_{24}Al_{28}O_{66}$). The cage centre oxygen ion is marked as O^*.

One attractive feature of the mayenite lattice is the ability to incorporate a multiplicity of foreign anions like halides (F^-,[6] Cl^-,[6-9]), oxygen species (O^-,[10, 11] O_2^-,[11, 12] O_2^{2-},[13] OH^-,[14-16]), small molecules (CN^-,[17] C_2^{2-},[18] NH_2^-,[19, 20] NO_2^-,[21] hydrazide $N_2H_{3-x}^{(1+x)-}$,[21]), sulphide S^{2-},[1] nitride N^{3-},[19, 20] hydride H^-,[22-24] and even electrons.[25-27] Beside the academic interests this unique property opens the possibility to develop new kinds of anion electrolytes[7, 17] as potential functional material for sensors,[9, 28] fuel cells, electronic devices[29-31] or ion emitters.[8, 12, 32-34] Additionally, Dong *et al.* were able to prepare an anion and cation substituted Sr-mayenite ($Sr_{12}Al_{14}O_{32}$:Cl_2) and reported on high humidity-sensitive ionic conduction (protons) at ambient temperature.[35] However, for all these applications typically a minimum conductivity and thermodynamic stability of the material is needed – and it is the purpose of the current paper to provide this fundamental information for a number of new phases.

Only few reports by Schmidt *et al.* (Cl^-, CN^-),[7, 17] Strandbakke *et al.* (OH^-)[16] and Hosono *et al.* (OH^-, O^-)[11] consider the mobility of foreign ions in mayenite. In this study we therefore explore the conductivity of less common anion-substituted mayenite phases, namely $C_{12}A_7$:X with X = F, S, N (notation: e.g. $Ca_{12}Al_{14}O_{32}$:F is abbreviated as $C_{12}A_7$:F ; note: the species right of the colon is located in the cage centre). From the obtained data we evaluate the possible utilisation of anion substituted mayenites as new kind of anion electrolytes.

In addition to anion substitution the influence of water on the mayenite phase will be addressed in detail, as there is contradictory evidence in literature for the formation and stability of mayenite under certain thermodynamic conditions. Kohatsu *et al.* successfully synthesized mayenite under dry atmospheres[36] whereas Nurse *et al.* reported that "anhydrous" C12A7 is not

stable in the $CaO–Al_2O_3$ system.[37, 38] Singh and Glasser[14] performed hydration and dehydration by using thermogravimetry and found almost complete reversible uptake and release of water based on the stoichiometric $Ca_{12}Al_{14}O_{33}(OH)_2$. Irvine and West[28] were the first to measure conductivity of mayenite under different humidity and temperature conditions and even proposed mayenite as moisture sensor. After hydration they were able to recover the original conductivity by heating to ~1350 °C. Hallstedt[39] performed theoretical calculations on the thermodynamic properties of the quasi-binary system $CaO–Al_2O_3$ and consider mayenite without incorporated water to be stable up to 1722 °C which was found to be its melting point. In contrast, Palacios *et al.* reported about the decomposition of mayenite at 1100 °C under dry reducing conditions and conclude that mayenite was not stable in the absence of any "template" cage ions (O^{2-}, OH^-, F^-).[40]

The hydration and dehydration of mayenite has already been examined by thermogravimetry,[14, 15] conductivity measurements,[9, 16, 28, 41] and IR spectroscopy.[15] The first microscopic description of the hydration process was proposed by Hayashi *et al.*[15]. A first point defect based model for this reaction was developed by Lee *et al.*[41] and Strandbakke *et al.*[16]. However, the validity of this model has not yet been verified in the entire accessible range of water partial pressure pH_2O. Therefore, the conductivity of O-mayenite has also been measured as function of temperature ($1000\ °C \leq \theta \leq 1200\ °C$) and pH_2O in the range of $-5 \leq \lg[pH_2O/\mathrm{bar}] \leq -1.6$.

Unfortunately, in some previous studies on mayenite no attention was paid to the experimental determination of water vapour pressure, which makes a judgement of the validity difficult. Often

the observation times of the mayenite phases under the respective thermodynamic conditions are not reported. Since Ca diffusion is required for the formation or decomposition of mayenite – which is comparably slow – long reaction times are required and decomposition could then be overlooked. A dedicated experimental study on the stability of O-mayenite under defined conditions is still missing. Therefore, we investigate the thermodynamic stability of mayenite with conductivity measurements and Raman spectroscopy in the present paper.

2. Charge transport and defect chemistry in dependence of water vapour pressure

Ionic charge transport in O-mayenite is substantially different from that in most solid ion conductors (e.g. YSZ). Oxygen ion migration can take place *via* oxygen interstitials (cage oxygen ions) O_i'' and framework oxygen vacancies $V_O^{\bullet\bullet}$. There are three possible migration mechanisms (**Figure 2**)[11, 19, 41, 42]: (a) A cage oxygen ion O_i'' kicks an adjacent framework oxygen O_O^x into an empty cage V_i^x while it itself takes the place of the displaced framework oxygen ion inside the framework (interstitialcy mechanism); (b) A cage oxygen ion O_i'' moves directly into a neighbouring empty cage site V_i^x through the opening of a cage wall by perpendicular displacement of framework ions (interstitial mechanism); (c) A framework oxygen ion O_O^x jumps into a framework oxygen vacancy $V_O^{\bullet\bullet}$ (vacancy mechanism).

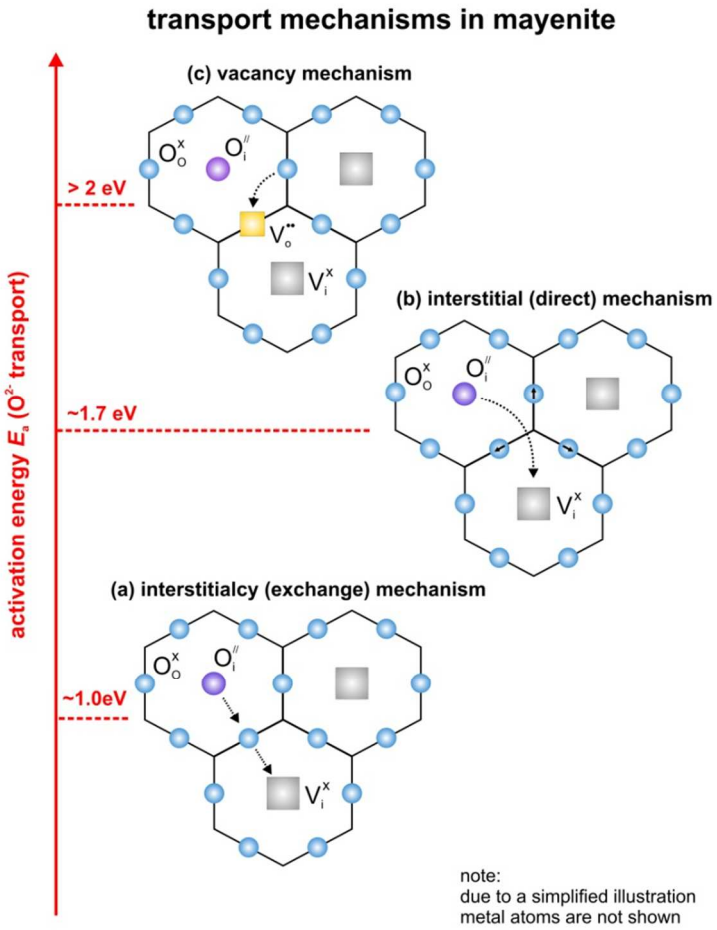

Figure 2. Possible oxygen ion transport mechanisms in mayenite and their energetic location in comparison to each other.

It has been shown by theoretical calculations that the interstitialcy mechanism is favoured for oxygen migration[11, 43]. The two other mechanisms are unlikely, as they require to overcome high activation barriers. Experimental evidence for mechanism (a) was obtained from isotope exchange experiments followed by Raman spectroscopy.[11, 44] After a certain time of thermal annealing in ^{18}O atmosphere the cage oxygen as well as the framework oxygen was partially replaced by ^{18}O with almost equal concentrations, which implies a fast exchange between cage and framework oxygen. Neutron powder diffraction experiments carried out by Boysen *et al.* confirmed these findings.[19, 42]

The transport of foreign cage ions apparently does not take place via the energetically favoured interstitialcy mechanism, as it would require the incorporation of the foreign ions into the cage walls, which is energetically not favorable. Indeed it was shown for Cl-mayenite that the interstitial mechanism which much higher activation energy occurs.[7] The total conductivity is given as

$$\sigma = \sum_i \sigma_i \ , \tag{1}$$

with

$$\sigma_i = \beta \times z_i \times e \times \mu_i \times [i], \tag{2}$$

where σ_i denotes the partial conductivity, z_i the charge number, μ_i the electric mobility and $[i]$ the concentration per formula unit of species i (e.g. O^{2-}, OH^-, Cl^-, F^-, e^-, ...) , β the molecular density ($\beta = \frac{N_A}{V_m}$, number of formula units per cm^3, with N_A and V_m as Avogadro's constant and molar volume) and e the elementary charge. For high oxygen activities (as of present concern) the electronic contribution to the total conductivity can be safely neglected[41].

As hydrated oxide,[45, 46] mayenite provides a "twofold" defect chemistry in the sense that it depends on both, the oxygen partial pressure pO_2 and the water vapour partial pressure pH_2O .[15, 16, 41] The resulting Brouwer-diagram $\lg[\text{def}]$ vs. $\lg p(g), g = O_2, H_2O)$ therefore has three dimensions which makes the defect chemistry of mayenite rather complex. In order to investigate the hydration of mayenite at high (and constant) oxygen partial pressure we limited our study to the pH_2O dependence. The pO_2 dependence has been studied in earlier reports.[16, 41]

The hydration of mayenite can formally be described using Kroeger-Vink notation (as used in Lee *et al.*[41]):

$$H_2O(g) + O_i^{//} + V_i^x = 2OH_i^{/} \quad (3)$$

The resulting law of mass action is then given as

$$K_h = \frac{\left[OH_i^{/}\right]^2}{\left[O_i^{//}\right]\left[V_i^x\right] pH_2O} . \quad (4)$$

Irvine and West[28] reported that water uptake leads to a decreased conductivity due to the formation of immobile hydroxide species. The diffusion coefficient of hydroxide ions was estimated to be roughly two orders of magnitude lower than that of oxide at 1000 °C.[15] One has to note that for one molecule of incorporated water the equal amount of cage oxygen $O_i^{//}$ is consumed which implies a decreasing charge carrier concentration and blocking of migration pathways by less mobile hydroxide ions. For high degree of hydration, the concentrations of $OH_i^{/}$ and V_i^x can be considered as constant and the cage oxygen concentration $\left[O_i^{//}\right]$ becomes proportional to pH_2O^{-1}. Protons appear to have a very low mobility in mayenite. [47]

Hayashi *et al.* proposed a hydration mechanism, which proceed in three steps: (a) Diffusion of $O_i^{//}$ to the surface, (b) reaction of $O_i^{//}$ with adsorbed water according to Equation (3), (c) inward diffusion of $OH_i^{/}$, being the rate determining step.[15] The net reaction represents the chemical diffusion of H_2O into the bulk of mayenite.

3. Experimental Section

3.1. Preparation and phase analysis of anion-substituted mayenite

Substituted mayenite with different cage anions was prepared by conventional high temperature solid state reaction according to the following steps:

O-mayenite

For the synthesis of O-mayenite ($Ca_{12}Al_{14}O_{33}$), a stoichiometric mixture of $CaCO_3$ and α-Al_2O_3 with a ratio of 12:7 was grinded in an agate mortar and then heated at a temperature of 1400 °C for 16 h in a chamber furnace. Afterwards it was grinded a second time and reheated for another 16 h at 1400 °C. Pellets for conduction measurements were obtained by uniaxial pressing the powder and sintering it at 1200 °C for 12 h in air (sample #1, 4, 5). Humidity was not controlled but corresponds to ambient conditions (~50% relative humidity at 25°C, approx. 18000 ppm H_2O). For comparison, a further sample of polycrystalline O-mayenite (sample #2) was prepared by a slightly different method (precursor for single crystal growth).[48] Additionally, single crystals were grown by floating zone method (sample #3).[48]

F-mayenite

F-mayenite ($Ca_{12}Al_{14}O_{32}:F_2$) was obtained by grinding a mixture of $CaCO_3$, α-Al_2O_3 and CaF_2 in a ratio of 11:7:1. The mixture was then heated in a chamber furnace for 16 h at 1200 °C. It was then grinded and heated under the same conditions for a second time. Pellets for conduction measurements were obtained as described for O-mayenite.

Cl-mayenite[7]

The preparation of Cl-mayenite ($Ca_{12}Al_{14}O_{32}:Cl_2$) was quite similar to that of F-mayenite. Instead of CaF_2, $CaCl_2$ was used. The first heating-step was carried out at 1050 °C for 16 h, the second at 1200 °C for 24 h.

S-mayenite

Sulfide containing S-mayenite ($Ca_{12}Al_{14}O_{32}$:S) was synthesized by mixing CaO, α-Al_2O_3 and CaS (11:7:1) in argon atmosphere. CaO was prepared in a previous step by heating $CaCO_3$ to 1200 °C in air for 16 h. The mixture was sealed in a tantalum ampoule and heated to 1400 °C under argon for 4 h.

CN-mayenite[17]

CN-mayenite $Ca_{12}Al_{14}O_{32}$:$(CN)_2$ was synthesized using a solid-gas reaction. CaO, α-Al_2O_3 and AlN (12:6:2) were mixed and pressed into pellets. The reaction was performed in a graphite-heated resistance furnace at a temperature of 1200 °C for 4 h, following equation:

$$12\ CaO + 6\ Al_2O_3 + 2\ AlN + 2\ CO \rightarrow Ca_{12}Al_{14}O_{32}(CN)_2 \quad (5)$$

Carbon monoxide was formed *in situ* from carbon dioxide impurities in CaO and carbon of the furnace.

N-mayenite

After treating O-mayenite with gaseous ammonia, different anionic nitrogen species like nitride (N^{3-}), amide (NH_2^-) and hydrazide ($N_2H_{3-x}^{(1+x)-}$) can be observed simultaneously. Nitrogen-modified mayenite is therefore denominated as N-mayenite or in case of partial substitution as N/O-mayenite[19-21, 49]. For preparation, O-mayenite was dried in a tube furnace under argon for 30 minutes at 1050 °C. The gas atmosphere was then switched to ammonia (15 L/h), which was led directly onto the sample via a special supply tube. The reaction was continued for further 16 h.

X-ray powder diffraction was performed to determine the crystallographic phase of the obtained anion substituted mayenite (PANalytical X'Pert Pro MPD). The diffractometer worked

in common Bragg-Brentano geometry with θ-θ-configuration and was equipped with a copper X-ray tube (λ_1 = 154.056 pm, λ_2 = 154.431 pm, I (λ_2/λ_1) = 0.5), a nickel filter and a Si(-Li)-semiconductor as detector. The lattice parameter and the occupation number of the cage anion species were obtained by Rietveld refinement (FullProf).

The anion elemental composition was examined by two different methods. Hot gas extraction (HGE) was used to determine the contents of N (LECO EF-TC 300 and TC400) C, H (Thermo Finnigan Flash EA 1112 NC) and S (LECO CS230) with an accuracy of $\pm 0.1\%$. The sample amount was approx. 500 mg. Additionally, Cl and S contents were measured by energy-dispersive X-ray spectroscopy (EDX, Hitachi S-2700). The cation content was taken from the ideal stoichiometry of O-mayenite.

The described method is not quantitatively reliable for the determination of such small amounts of hydrogen as present in the samples. Therefore, the obtained results have to be considered as approximate values.

3.2. Raman spectroscopy

In addition to the routine XRD crystal structure analysis Raman spectroscopy offers high sensitivity for probing local as well as long range symmetry in both, the anion and cation sublattice. Raman spectroscopy was carried out on pristine sample pellets and degraded sample bars (after conductivity experiments) at room temperature in air with a Bruker Senterra Raman Microscope. The excitation source was a green Ar laser with a wavelength of 532 nm. A power rating of 2 mW was used.

3.3. Electrical conductivity

To examine the transport properties and the anion mobility in anion-substituted mayenite, measurements of the total conductivity were performed in a temperature range of $600 \leq \theta / °C \leq 1200$ at different humidity. Thus, the as prepared sample pellets were cut into rectangular bars with dimensions of approx. 1x1x4 mm³. The exact dimensions were measured with a digital sliding calliper. Platinum paste (Ferro No. 64021015 Pt paste, Hanau, Germany) was painted on both end faces of the bars and dried in air for improved electrical contact. The samples prepared in this way were then mounted onto a sample holder inside a gastight high temperature tube furnace. In between two parallel platinum electrodes the samples were fixed with a light spring pressure applied by an alumina tube.

Experiments were performed under a streaming gas flow of 100 cm^3/min. Predried and humidified gases (air, Ar, O_2) were mixed in the required ratios, depending on the experimental conditions. The predried gases were prepared by streaming first through $CaCl_2$ granulate and afterward through P_2O_5 (SICAPENT drying agent, Merck KGaA, Germany). With this procedure a residual humidity of less than 1 ppm H_2O was achieved. Humidification was carried out by leading the gas stream through a water filled bubble counter. The upper limit is marked by ~100% rh (relative humidity) at room temperature which corresponds to ~3.5% (35000 ppm) absolute humidity. The humidity a the sample was taken as the value measured downstream (behind the sample furnace) by two different humidity sensors, depending on the respective range (3.5 % – 0.05 %, Hygrochip HYT-939, IST AG, Switzerland; 500 ppm – 1 ppm, AMT-SP, PRO-CHEM Analytik, Germany).

The electrical resistance was measured via impedance spectroscopy in two terminal setup with an EG&G potentiostat (model 283) equipped with a PAR model 1025 frequency response analyzer. A frequency range of $500\ \text{kHz} \geq f \geq 100\ \text{mHz}$ and an excitation amplitude of 100 mV was used. The sample was allowed to equilibrate at the given thermodynamic conditions for at least 4 h until the measurement was started. Evaluation of the obtained impedance spectra was done with the program package PowerSine.

Alternatively, for isothermal kinetic experiments (humidity equilibration) and experiments under varying humidity, a fast 2-point DC measurement was deployed. Different currents were drawn consecutively across the sample (Keithely 224 current source) while the respective voltages were recorded (Keithley 6517A electrometer). The slope of the *U*-*I*-characteristic yields the sample resistance.

Finally, the total conductivity was calculated with the sample dimensions according to

$$\sigma = \frac{l}{A \times R}, \tag{6}$$

where σ denotes the total conductivity, l the electrode distance (sample length), A the electrode cross section area and R the measured sample resistance.

4. Results and Discussion

4.1. Crystal structure and composition of anion-substituted mayenite

The phase identity of anion substituted mayenite was determined by x-ray diffraction. For all substituted samples the pure mayenite phase was obtained. An exemplary diffraction pattern of S-mayenite is illustrated in **Figure 3**. The quality of the refinement is quite well ($R_{\text{Bragg}} = 0.044$; $R_{\text{wp}} = 0.079$; $R_{\text{exp}} = 0.021$; $S = 3.8$). The lattice parameters are close to each other while a slight

increase in the order F, O, S, Cl, N to CN can be observed (**Table 1**). Thus, the cage anions seem to have a significant effect on the density of mayenite.

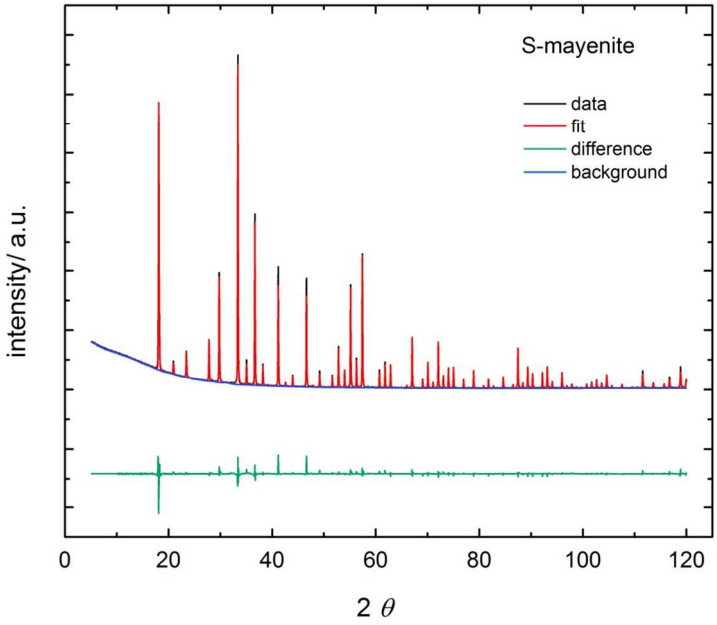

Figure 3. Diffraction pattern of S-mayenite refined with FullProf.

Not surprising, F-mayenite exhibits the smallest lattice parameter of a = 1197.10 pm, which is in good agreement with previous reports[6]. In addition, the occupation number for the cage center position (3/8 0 1/4) was found to be higher than in O-mayenite. As 1/3 of the cages instead of 1/6 are occupied, this result is expected.

Table 1. Results of structural and compositional characterisation of $C_{12}A_7$:X

sample / X	nominal elemental formula	lattice parameter a / pm	anion content wt.-% nominal	anion content wt.-% measured	achieved elemental formula
O	$Ca_{12}Al_{14}O_{32}$:O	1198.50	-	-	-
F	$Ca_{12}Al_{14}O_{32}$:F_2	1197.10	2.70	-	-
Cl	$Ca_{12}Al_{14}O_{32}$:Cl_2	1200.72	4.92	4.7	$Ca_{12}Al_{14}O_{32}$:$Cl_{1.9}O_{0.05}$
S	$Ca_{12}Al_{14}O_{32}$:S	1200.38	2.29	1.92 (EDX) 2.0 (HGE)	$Ca_{12}Al_{14}O_{32}$:$S_{0.84}$ $O_{0.16}$ $Ca_{12}Al_{14}O_{32}$:$S_{0.87}$ $O_{0.13}$
CN	$Ca_{12}Al_{14}O_{32}$:$(CN)_2$	1204.08	C: 1.69 N: 1.97	C: 1.58 N: 2.10	$Ca_{12}Al_{14}O_{32}$:$C_{1.87}N_{2.13}$ O_x
N	(see text, Section 4.1)	1201.30	-	N: 2.14 H: 0.07	$Ca_{12}Al_{14}O_{32-x}$:$N_{2.14}H_{0.96}$

Elemental analysis was performed only for Cl, S, C, N and H. The residual unsubstituted cage oxygen was not determined. It was expected to add up such as the charge neutrality condition is obeyed. The elements behind the colon mark their location in the cage center.

Cl-mayenite agrees with literature reports[6] as well and a recent neutron powder investigation[7] revealed the occupation number of chlorine in the cages to be close to the theoretical value of $n(\mathrm{Cl}) = 0.083$ within an error margin of two sigma. Concerning CN-mayenite, the occupation numbers of both, C and N in the cages were found to be $n = 0.0818$, a value close to the theoretical value of $n(\mathrm{CN}) = 0.0833$.[17]

Elemental analysis was carried out for Cl-, S-, CN-, and N-mayenite (**Table 1**). For all investigated samples the theoretical compositions were almost achieved. In case of Cl- and S-mayenite only a small fraction of cage oxygen remained unsubstituted. Concerning CN-mayenite, the ratio of $[\mathrm{C}]/[\mathrm{N}] = 0.88$ and the nitrogen concentration $[\mathrm{N}] = 2.13$ implies a small excess of nitrogen. Since the exact species of this excess nitrogen is unknown, the residual oxygen cannot be calculated.

The stoichiometry of N-mayenite is rather speculative, since different kinds of nitrogen species (nitride, amide, hydrazide) inside the structure have been observed.[19, 21, 42, 49] A first

spectroscopic prove (XPS) for the simultaneous presence of both N^{3-} and NH_2^- was given by Polfus *et al.*[20]. A large amount of nitrogen and hydrogen in our sample is therefore not surprising. The ratio of $[N]/[H] \approx 2$ with an excess of nitrogen reveals that N^{3-} and NH_2^- are most probably present at once. Furthermore, Polfus *et al.* also suggest based on theoretical calculations that N^{3-} substitutes oxygen in the framework, written as $N_O^{/}$, whereas NH_2^- is located in the cage centre, then written as $(NH_2)_i^{/}$. They propose the general formula $Ca_{12}Al_{14}O_{31}N_x:(NH_2)_x\,O_{0.5-0.5x}$ but with a restriction of a maximum nitrogen content of 50% which leads to a stoichiometry of $Ca_{12}Al_{14}O_{31.5}N_{0.5}:(NH_2)_{0.5}\,O_{0.5}$. Since N^{3-} is thought to be located in the framework rather than in the cage centre the electroneutrality condition $2[O]_{FW} = [N_O^{/}] + [(NH_2)_i^{/}] + 2[O_i^{//}]$ becomes crucial in the picture of a pseudo-donor model[41]. Transferring these considerations to the present case results in the stoichiometry of almost exactly $Ca_{12}Al_{14}O_{30.5}N_{1.5}:(NH_2)_{0.5}$ and in an expanded general formula of $Ca_{12}Al_{14}O_{32-y}N_y:(NH_2)_x\,O_{1-0.5(x+y)}$ with x and y depending on the respective hydrogen and nitrogen content (limits: $x+y \leq 2$). Obviously, a higher nitrogen content was achieved in the present work compared to previous reports.

On the contrary, in our recent studies no framework nitrogen could be detected by refinement of neutron powder diffraction data (on the same sample as in this work). [21, 42] One has to note, that O and N can be very well distinguished in neutron diffraction, thus, this results appears o be quite reliable. Furthermore the nitrogen content, when considering only framework nitrogen $[N_O^{/}]$, is limited to 2.05 wt.-% ($Ca_{12}Al_{14}O_{30}N_2$), but a higher amount of up to 4.5 wt.-% was

found. Schmidt *et al.*[21] proposed small amounts of hydrazide species ($N_2H_{3-x}^{(1+x)-}$) inside the cages at very high nitrogen contents (>2 wt.-%).[21] However, the experimentally determined ratio of $[N]/[H] \approx 2$ points towards additional nitrogen-rich species (i.e. N^{3-}) inside the cages. Uncertainties in the hydrogen determination (see Section 3.1) unfortunately do not permit the calculation of exact fractions of amide NH_2^-, nitride N^{3-} and hydrazide $N_2H_{3-x}^{(1+x)-}$ within the cages. Especially the total amount of charges carried by the anions remains unclear and may be compensated by additional framework oxygen vacancies. The sum formula is therefore proposed as $Ca_{12}Al_{14}O_{32-x}:N_{2.14}H_{0.96}$ without taking care of the individual species.

Raman spectroscopy was performed in addition to X-ray diffraction to complement the results on the phase identity of anion-substituted mayenite (**Figure 4**). Mayenite exhibits several modes in the range of 150-1000 cm^{-1} which are assigned to Al-O framework vibrations. The most dominating mode at 520 cm^{-1} is attributed to a symmetric Al-O-Al vibration of the bridge oxygen between AlO_4 tetrahedrons[50]. Modes located at 770 cm^{-1}, 880 cm^{-1} and 910 cm^{-1} arise from Al-O stretching vibrations within AlO_4 tetrahedrons[50]. The group of weaker modes which appears between 150 cm^{-1} and 400 cm^{-1} is assigned to doubly and triply degenerated framework oxygen.[44, 51] Especially S-mayenite shows two additional strong modes at 218 cm^{-1} and 637 cm^{-1} which origin remains unclear.

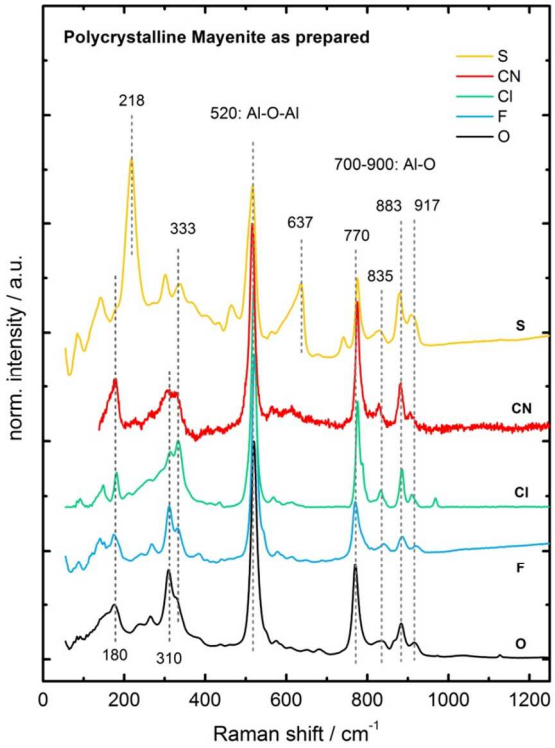

Figure 4. Raman spectra of the as-prepared anion-substituted mayenite samples.

The typical modes for the most common decomposition products of mayenite, namely CA, C_3A and C_5A_3, are missing (see **Table 3**) wherefore the prepared anion-substituted mayenite samples are considered as phase pure (refer to CCN, cement chemist notation, i.e. $C_xA_y = xCaO\ g\,yAl_2O_3$).

4.2. Total conductivity of anion-substituted mayenite

The electrical transport of foreign cage ions in mayenite has been studied by electrochemical impedance spectroscopy (EIS) in the temperature range of $600 £ \theta / °C £ 1000$. A typical impedance spectrum is shown in **Figure 5**. Only one single semicircle has been observed in the Nyquist representation (**A**). In terms of an electrical equivalent circuit and consistent with the

Bode representation (**B**) this frequency response is assigned to a parallel *RC*-circuit where *R* depicts the sample resistance and *C* the sample capacitance. In previous reports on mayenite more features were found in impedance spectra whereby grain boundary and bulk resistance could be distinguished.[4, 5, 52] In the present case with only one characteristic feature, the measured resistance represents a combined bulk and grain boundary resistance (refer to Section 4.3 for a detailed discussion). The time constants $\tau = RC$ of the charge transport processes within bulk and across grain boundaries appear to be close together (difference smaller than one order of magnitude), so that they cannot be distinguished, or one process strongly dominates the whole electric response. The dielectric constant ε, calculated as $\varepsilon = \frac{C}{\varepsilon_0} \times \frac{l}{A}$, presents a high value of 6×10^3 and therefore rather corresponds to gain boundary contribution in solid electrolytes. [53, 54]

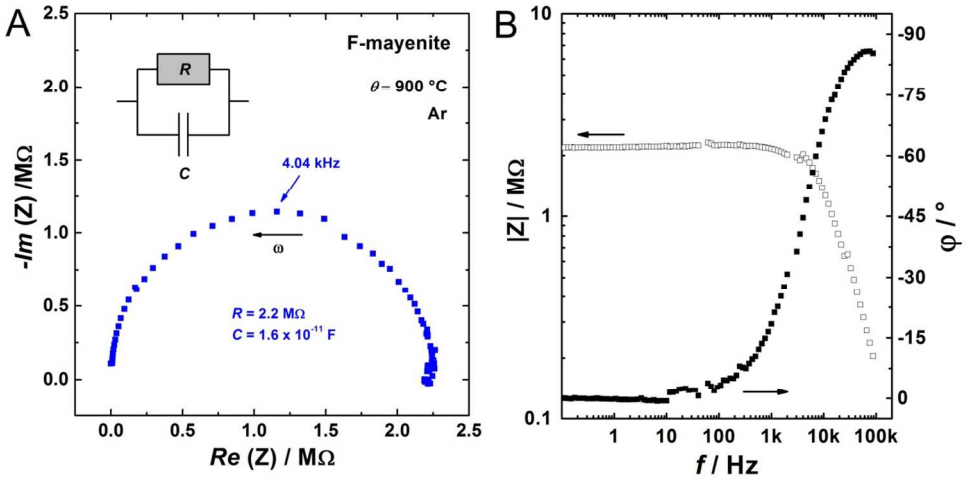

Figure 5. Typical impedance spectrum of mayenite in Nyquist (A) and Bode (B) representation.

To check whether the used two-terminal setup is valid for the mayenite electrolyte system, experiments with different sample connections were performed (**Figure 6**). Virtually no difference between both connections was observed. Parasitic disturbances from the cell

connection wires and possible high charge transfer resistances at the electrodes are therefore not expected. For simplicity sake, the two-terminal setup was applied to all further measurements.

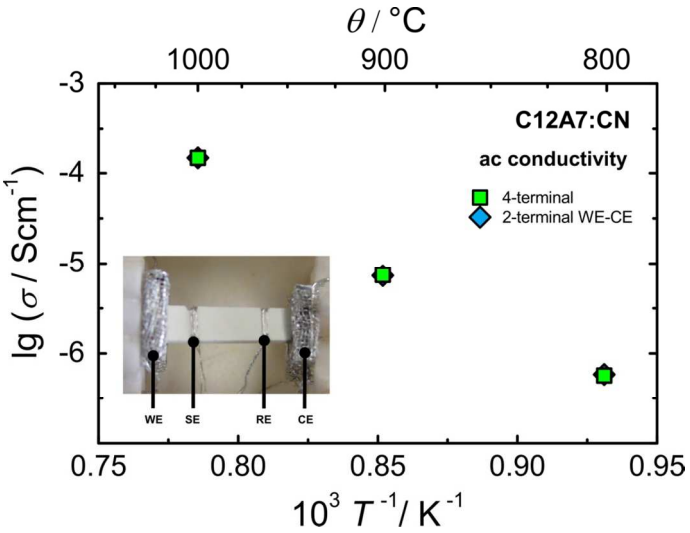

Figure 6. Comparison of two- and four-terminal electrical connection of the sample.

During preliminary experiments it turned out that some anion-substituted mayenite samples were not stable above 1000 °C under the given dry conditions (humidity < 10 ppm H_2O) at which decomposition of $C_{12}A_7$:CN and $C_{12}A_7$:N to C_5A_3 was observed. It was therefore decided to limit the temperature to 900 °C since decomposition was expected for other anion-substituted mayenites, too. The temperature dependence of the conductivity was then measured while heating up from 600 °C to 900 °C, holding this temperature for some time and by cooling down to 600 °C to prove the reversibility and/or possible changes of the samples (**Figure 7**). At first, one can notice a far lower conductivity and a much steeper slope of anion-substituted mayenite in comparison to O-mayenite. In addition, a hysteresis of the temperature dependence was found which may have two different origins: (1) Some mayenite samples may contain residual amounts of OH^- inside the cages due to the preparation process or sample storage. With increasing temperature this OH^- is replaced by traces of oxygen in the argon gas stream accompanied by an

increase in conductivity (refer to section 4.4). (2) Foreign cage anions decompose or are replaced by oxygen which results an increase in conductivity, too.

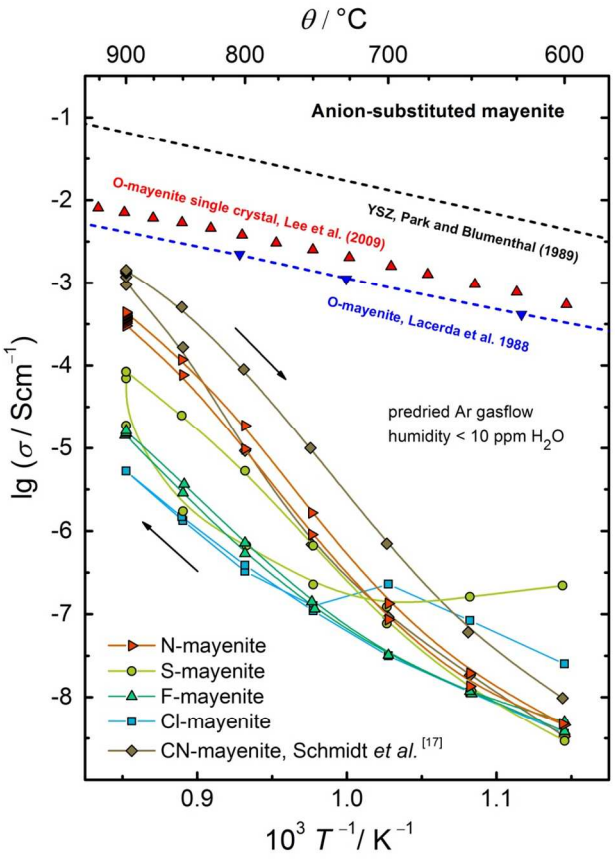

Figure 7. Total conductivity of anion-substituted mayenite as a function of reciprocal temperature. Solid lines are drawn to guide the eye.

Indeed there is some evidence for case (2) to occur; although the crystal structures after cooling down correspond to mayenite, the lattice parameters and occupation numbers of CN-, N- and S-mayenite more resemble to O-mayenite which provides an argument for a certain mobility of the cage anion species and hence a partial exchange with oxygen from the gas phase. Interestingly, the conductivity of CN-mayenite comes close to that of O-mayenite. Exceptions are Cl- and F-mayenite, where the cage anions appear to be stable and tight bound inside the cages.

The activation energy for the charge transport has been calculated from selected data points in the middle of the falling temperature branch after Equation (7):

$$\ln[\sigma T] = \ln \sigma_0 - \frac{E_a}{kT} \quad (7)$$

The results, summarized in **Table 2**, reveal a much higher activation energy than for O-mayenite and other oxygen ion conductors like YSZ (yttria-stabilized zirconia). The reason can be well found in the underlying transport mechanism as discussed in section 2, where other cage anions than oxygen cannot realize the energy favoured interstitialcy mechanism.[7, 17]

Table 2. Activation energy for the charge transport in anion-substituted mayenite and reference materials.

sample	E_a / eV
C12A7:CN, Schmidt *et al.*[17]	4.30 ± 0.09
C12A7:N	4.52 ± 0.13
C12A7:S	3.93 ± 0.04
C12A7:F	3.37 ± 0.10
C12A7:Cl	2.65 ± 0.10
C12A7:O, Lacerda *et al.*[5]	0.85 ± 0.01
C12A7:O single crystal, Lee *et al.*[41]	0.81 ± 0.01
YSZ, Park and Blumenthal[55]	0.87 ± 0.01

However, it cannot be ruled out that other mobile charge carriers partially contribute to the total conductivity. As mentioned above partially exchanged oxygen may increase the total conductivity as well as partial electronic conductivity – although the latter may be neglected, as we have no indication for reduction of the mayenite phases. In a previous study we estimated the transference number of electrons to be less than 0.1 in Cl- and CN-mayenite.[7, 17]

Additionally, the dependence of conductivity on the composition of Cl-mayenite, $Ca_{12}Al_{14}O_{32}:O_{1-x}Cl_{2x}$ $(0.0 \leq x \leq 1.0)$, was examined for different temperatures (**Figure 8**). The

total conductivity decreases monotonously with increasing Cl content. The effect is more pronounced at lower temperatures even at small concentrations of chlorine. These results underline the low mobility of Cl inside the mayenite structure and rather points toward a blocking character.

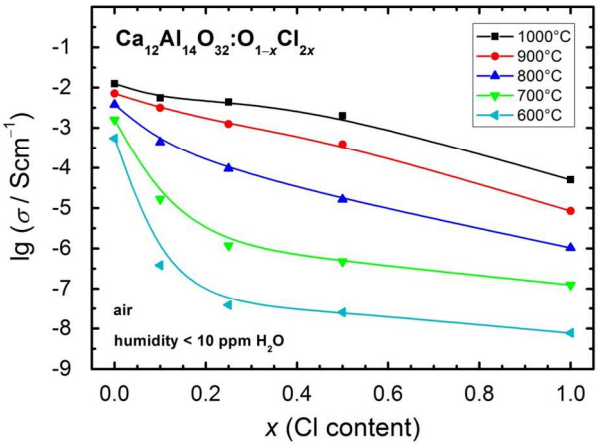

Figure 8. Total conductivity of Cl-mayenite as a function of Cl content *x* for different temperatures. Solid lines are drawn for a better visualisation.

4.3. Thermodynamic stability of O-mayenite in view of grain size, water vapour pressure and temperature

The conductivity of a solid is usually very sensitive to changes in its crystal structure and its composition, why it is well suited to probe the stability of mayenite under well-defined thermodynamic conditions. **Figure 9** presents the decomposition of different O-mayenite samples in dry atmosphere monitored by impedance spectroscopy during heat-up and cool-down. In the low temperature region (θ < 900 °C) in the heat-up branch one can notice a strong scatter of the conductivity between all samples and in comparison to the literature data. At first glance one might suspect whether this arises from different initial hydration states but the differences are too large for that effect solely. In some reports it was found that the conductivity of mayenite

is strongly affected by the preparation method, sintering time and sintering temperature. The grain boundary resistance appears to play a remarkable role.[4, 5, 52]

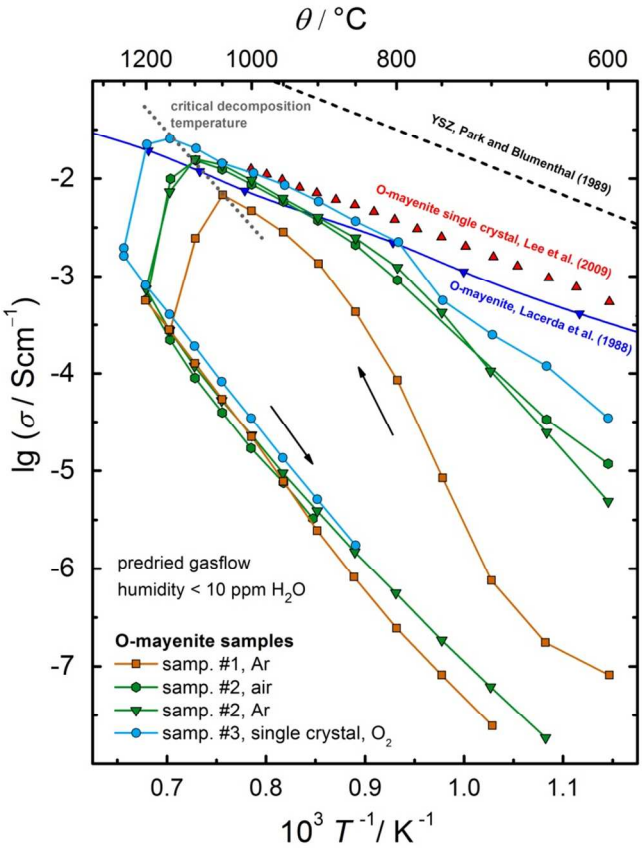

Figure 9. Decomposition of different O-mayenite samples in dry atmosphere monitored by impedance spectroscopy.

Evidence for a different mean grain size in the investigated polycrystalline samples gave the inspection by SEM. For sample #1 with the lowest conductivity a grain size of ~100 nm was roughly estimated whereas sample #2 showed larger grains of ~5 µm. Furthermore, sample #1 exhibits a diminished relative density of only 84% (calculated from sample mass and geometry). Sample #2 turned out to be almost fully dense within the experimental error. We assume that the grain boundary density and the relative sample density are responsible for the observed scatter in conductivity. Matsuda *et al.* found that the activation energy of the grain boundary transport is

approx. twice as high as for the bulk transport.[52] And in a previous study, Irvine *et al.* observed that the higher the temperature the smaller the grain boundary influence becomes.[4] Thus, the conductivities of the different samples converge with increasing temperature, and bulk conduction determines the course of the conductivity at high temperatures.

In the high temperature region (θ > 900 °C) the conductivity shows a sharp drop of about 1.5 orders of magnitude, but for each sample this drop occurs at an individual temperature. The initial high conductivity was never retained after cooling, therefore, the observed change in the conductivity has to be considered as irreversible.

The experiments clearly show that mayenite decomposes in dry atmosphere (less than 10 ppm H_2O) in the temperature range between 1050 °C and 1200 °C. In order to identify the stability limit as a function of humidity, a pristine mayenite sample (sample #5) was heated up to 1200 °C in wet atmosphere and was successively stepwise exposed to dry conditions (**Figure 10**). Above 150 ppm no change in resistance was observed within several hours. Below that value a slight increase occurred. The onset of a strong increase was found at about 70 ppm with a maximum of 83 kΩ at 20 ppm. The time scale of the decomposition reaction points to a very slow reaction which takes at least more than 36 h. Interestingly, switching back to wet conditions results in a decreasing resistance which implies a certain reversibility, although the initial resistance value was not reached even after 100 h.

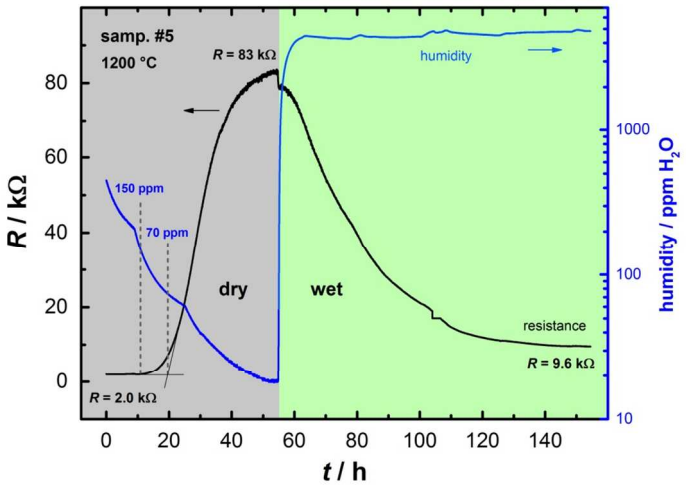

Figure 10. Decomposition of O-mayenite upon decreasing humidity monitored with DC resistance measurement.

In order to further investigate the formed phases after decomposition, Raman spectroscopy was used as diagnostic tool. Small changes in the local symmetry disturb the translational symmetry of the whole crystal, which results in a high sensitivity of this method for phase changes.

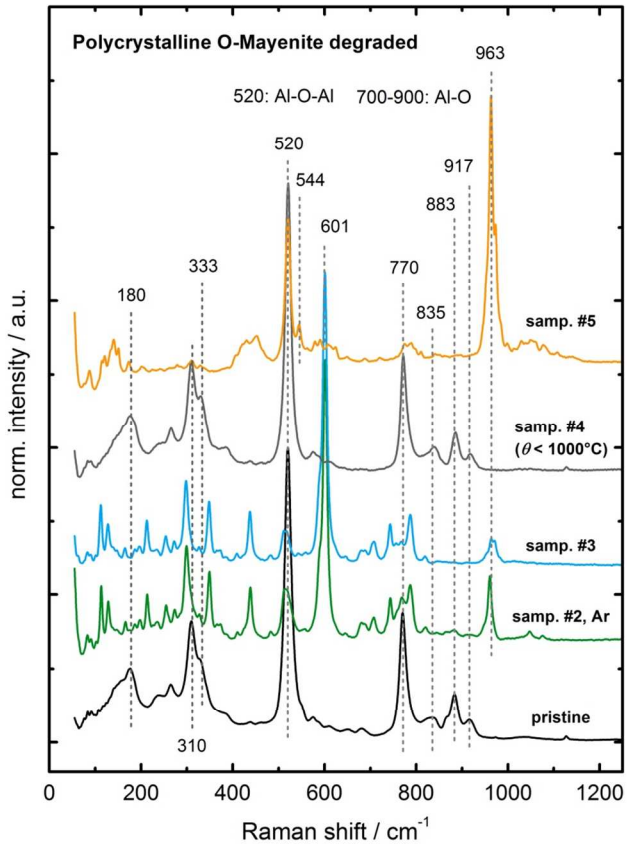

Figure 11. Raman spectra of degraded O-mayenite samples.

Figure 11 presents Raman spectra of degraded O-mayenite samples after the decomposition experiment (see **Figure 9**). A couple of new modes have formed with respect to the pristine sample which gives evidence for a loss in symmetry. Ruszak *et al.* investigated the pure calcium aluminate phases CA, C_3A, C_5A_3, and $C_{12}A_7$ with Raman spectroscopy and located modes for a definite identification of the respective phase (see **Table 3**).[51] Besides several modes of medium intensity, sample #2 and sample #3 show a sharp and intense mode at 601 cm^{-1} which can be assigned to C_5A_3. Obviously, for the degradation it does not matter whether Ar or air is present and if the sample was single or polycrystalline. Sample #4 was only exposed to 1000 °C and appears to fully retain the mayenite phase (confirmed with XRD after cooling down). The decomposition and partial recovery of sample #5 is presented in **Figure 10**. Raman spectroscopy

clearly proves that the mayenite phase is not retrieved after the final treatment in wet atmosphere. The main modes at 520 cm^{-1} and 544 cm^{-1} and the missing modes between 700 cm^{-1} and 900 cm^{-1} indicate the presence of CA. Nevertheless, the existence of small fractions of other calcium aluminate phases beside the main phases cannot be ruled out. All decomposed samples additionally exhibit a strong mode around 960 cm^{-1} which we were not able to assign safely to a unique phase.

Table 3 Raman modes for the identification of calcium aluminate phases after Ruszak *et al.*[51].

mode / cm^{-1}	phase			
312	$C_{12}A_7$			
333	$C_{12}A_7$			
508			C_3A	
521	$C_{12}A_7$	C_5A_3		CA
546				CA
600		C_5A_3		
756			C_3A	
772	$C_{12}A_7$			

In the following the decomposition of mayenite is discussed on the thermodynamic background of the calcium aluminate system. Studies on the formation of mayenite have shown that several phases are involved, depending on the experimental conditions. It was found that C_5A_3 was the intermediate product at temperatures up to 950 °C, whereas at higher temperatures C_3A and CA are the major intermediate phases (i.e. there appears to exist a high and low temperature formation process).[51] The decomposition might therefore take the same reaction pathways, albeit in the opposite direction.

In the phase diagram for humid conditions (**Figure 12**) mayenite is adjacent to C_3A and CA, and it forms a binary eutectic each with both phases at almost the same temperature. The

metastable phase C_5A_3 (refer to Nurse *et al.*[38]) is only slightly different in composition and is therefore very close located to $C_{12}A_7$. Decomposition of $C_{12}A_7$ occurs by a separation into a Ca-rich and into a Al-rich phase (i.e. into one phase left and one phase right with respect to mayenite). Under dry conditions mayenite is a metastable phase, and C_3A and CA become coexisting phase in a wide range of composition of the $CaO\text{-}Al_2O_3$ system (**Figure 12** inset). [38] On the basis of these findings two decomposition reactions are reasonable for the observed formation of C_5A_3 and CA:

$$4\ C_{12}A_7 \rightarrow 9\ C_5A_3 + C_3A \quad (8)$$

$$2\ C_{12}A_7 \rightarrow 9\ CA + 5\ C_3A \quad (9)$$

In both cases an additional minor phase of C_3A is formed which seems to be hidden in the respective Raman spectra below the modes of the major phases (see **Figure 11**); or it forms as amorphous phase.

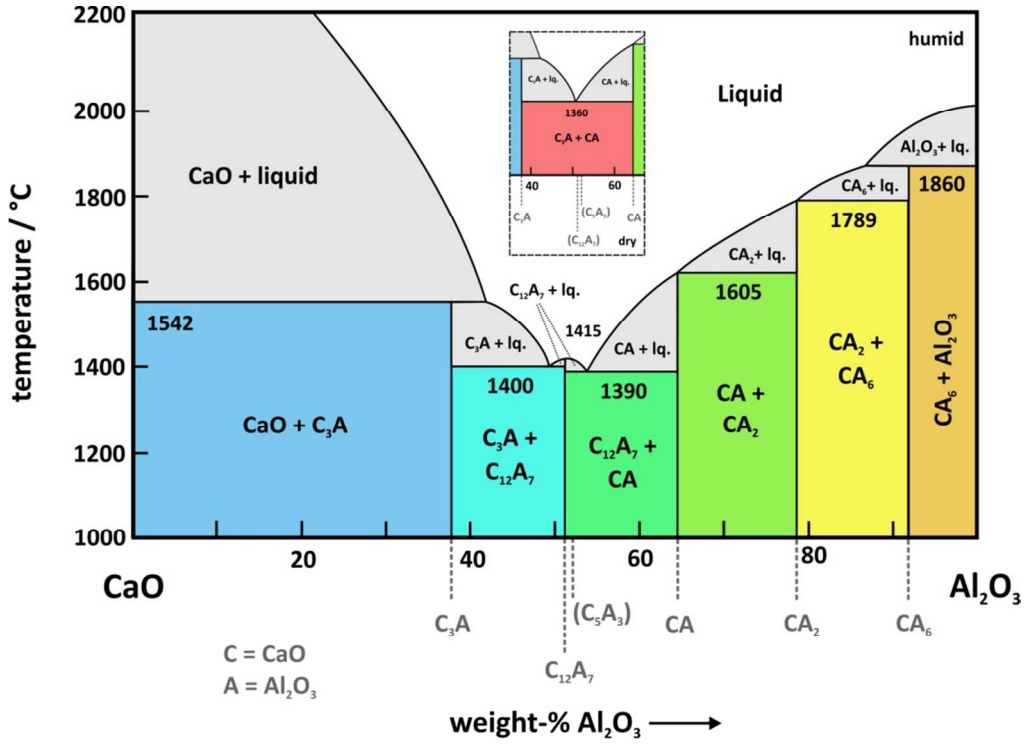

Figure 12. Calcium aluminate phase diagram for humid conditions redrawn after *Lea's Chemistry of Cement and Concrete*[3]. Inset: Section of the phase diagram around the $C_{12}A_7$ composition for dry conditions after Nurse *et al.*[37, 38] . Phases in brackets are considered as metastable.

We assign the degradation of samples #1–3 (**Figure 9**) to Equation (8), since predominantly C_5A_3 is formed. The different temperatures observed for the onset of the decomposition can be explained as follows: It has been reported that Ca ions are the main diffusing species[36, 51] during the formation of calcium aluminate phases, which is then also expected for their decomposition. Degradation will start at macroscopic crystal defects (e.g. grain boundaries, cavities) since there are more sites for the rearrangement of atoms available. Therefore, sample # 1 with the smallest grains (highest grain boundary density) and least sample density degrades at a lower temperature than the single crystalline sample #3, i.e. when the mobility of Ca is high enough for the short diffusion lengths in small grains. As mentioned above, in case of C_5A_3 as decomposition product

only a slight shift in composition starting from $C_{12}A_7$ is needed. So, the decomposition according to Equation (8) is a comparably fast process (few hours). During the experiments dry conditions were established before the temperature was increased. This obviously favored the low temperature route via C_5A_3 as already observed during the mayenite formation reaction.[51]

Different from the usual procedure, the temperature was first set to 1200 °C before the humidity was consecutively lowered during the degradation experiment of sample #5. This approach led to a reaction pathway via C_3A and CA (Equation 9) as found in the high temperature formation route[51]. Since a more severe change of local composition is required for this route, this degradation process is much slower and needs time in the order of days to expire.

The results of the present observations lead to one major conclusion: Mayenite is not stable in dry atmospheres as it was already reported in some earlier studies – but which has been often forgotten since. Hydroxyl anions inside the mayenite cages appear to have a significant stabilization effect and a strong impact on the total conductivity. At temperatures below the critical mobility limit of Ca ions (θ < 1050 °C) mayenite is kinetic stabilized and therefore metastable, in particular in case of coarse-grained or single crystalline materials. The reason why mayenite was frequently reported to be stable in dry atmospheres may simply arise from too short exposure and observation times since Ca diffusion in mayenite is a slow process.

4.4. Conductivity and defect-chemistry of O-mayenite in dependence of $p(H_2O)$

In order to further investigate the defect chemistry upon hydration and the hydration mechanisms of mayenite, electrical conductivity measurements as function of water vapour partial pressure $p(H_2O)$ at temperatures of 1000 °C £ θ £ 1200 °C were performed (**Figure 13**).

All conductivity isotherms show a uniform and consistent course with a slope of –1 in the high water vapour pressure regime (cf. section 2). Upon decreasing $p(H_2O)$ all curves bend down and approach a limiting value. The highest conductivity values are obtained at 1200 °C.

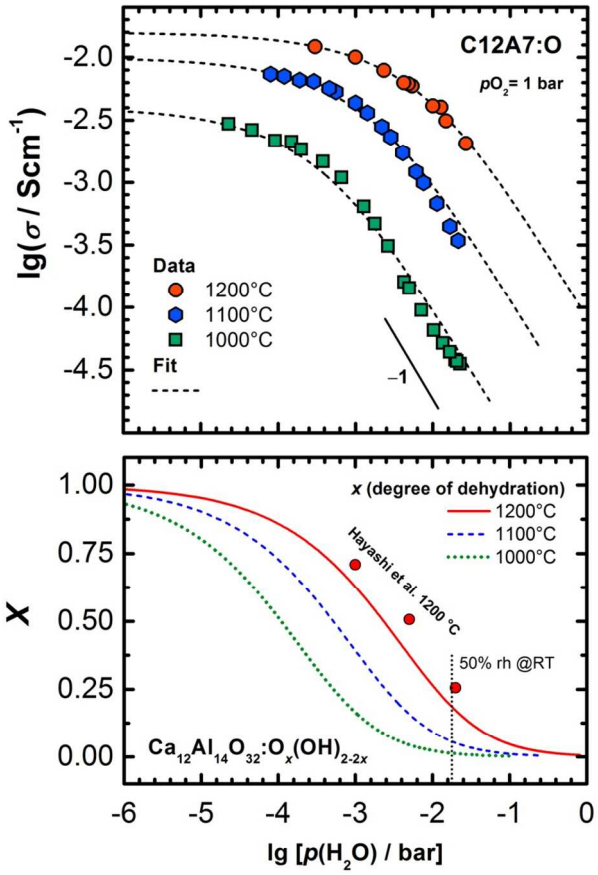

Figure 13. Conductivity and hydration of mayenite as a function of water vapour partial pressure. For comparison reference data of Hayashi *et al.* measured with IR spectroscopy was included.[15] The dotted line marks the point of 50 % rh (relative humidity) at room temperature which is close to ambient conditions.

The shape of the isotherms reminds of curves obtained for oxygen non-stoichiometry δ as function of oxygen partial pressure $p(O_2)$ in transition metal oxides (e.g CeO_2).[56, 57] Therefore, a modified approach as normally used to fit the course of δ vs. $p(O_2)$ is applied to O-mayenite to

describe the hydration in dependence of water vapour pressure (thereby extending the defect-chemical approach in Lee *et al.*[41]).

We consider $Ca_{12}Al_{14}O_{32}:O_x(OH)_{2-2x}$ to describe O-mayenite in the hydrated state and x be the non-stoichiometry in OH^- (degree of dehydration). According to the site balance

$$[O_i''] + [OH_i'] + [V_i^x] = 6, \quad (10)$$

the sum of all occupied and unoccupied cage sites has to add up to 6 (six cage per formula unit of mayenite). As a further restriction the charge neutrality condition

$$2[O_i''] + [OH_i'] = 2, \quad (11)$$

has to be obeyed (two excess charges per formula unit of mayenite). Now, Equation (10) and (11) can be solved partially to express $[OH_i']$ and $[V_i^x]$ by $[O_i'']$:

$$[OH_i'] = 2 - 2[O_i''] \quad (12)$$

$$[V_i^x] = 4 + [O_i''] \quad (13)$$

The nonstoichiometry variable x can be expressed as $x = [O_i'']$, and obeying Equation (12) and (13) the law of mass action for hydration (Equation 4) can be formulated to give

$$\lg pH_2O = -\lg K_h + \lg\left[\frac{(2-2x)^2}{x(4+x)}\right]. \quad (14)$$

Since we have no direct access to the nonstoichiometry variable x it is substituted by the conductivity: We assume the mobility of the hydroxide ions to be small compared to the oxygen ions and proton conduction to be negligible (both has already been demonstrated[15]). Thus, the total conductivity vs. $p(O_2)$ is dominated by oxygen ion conductivity ($\sigma = \sigma_O$). Then, Equation (2) can be solved for the charge carrier concentration $[O_i'']$:

$$\left[V_O^{\bullet\bullet}\right] = \frac{\sigma_O}{\beta \cdot 2 \cdot e \cdot \mu_O} \tag{15}$$

If the oxygen ion mobility μ_O is considered to be constant with respect to $p(H_2O)$ the denominator may be expressed by a constant factor K_μ as

$$\left[V_O^{\bullet\bullet}\right] = \frac{\sigma_O}{K_\mu} = x\,. \tag{16}$$

Then, Equation (16) is inserted into Equation (14) and fitted to the experimental data ($\lg p\mathrm{H_2O}$ vs. σ) with K_h and K_μ as free parameters (**Table 4**). The agreement with the measured course of the conductivity isotherms is quite well (**Figure 13**, dashed lines). According to Equation (16), the degree of dehydration *x* was calculated from σ_O and K_μ, and plotted against the water vapour partial pressure. As expected, dehydration is more pronounced at higher temperatures and only significant in predried atmospheres. In the converse argument, O-mayenite synthesized in ambient atmosphere resembles more likely a mixed OH^- and O-mayenite[16]. This explains well why a strong dependence of the conductivity on the sample history and the preparation conditions was found.[5] In comparison with a previous report by Hayashi *et al.* there is only a slight deviation, which is most probably due to the different measurement techniques.[15]

Table 4. Fit results for hydration of O-mayenite after Equation (14).

θ / °C	K_h	K_μ
1200	$1.9 \cdot 10^2$	0.016
1100	$8.6 \cdot 10^2$	0.010
1000	$4.1 \cdot 10^3$	0.004

From the fitted values for K_h the thermodynamic parameters $\Delta_h H^0$ and $\Delta_h S^0$, the standard enthalpy and entropy of hydration were determined: The relation between the equilibrium constant of a reaction and the standard Gibbs free energy is given as

$$\ln K = - \frac{\Delta_r G^0}{RT}. \quad (17)$$

In combination with Gibbs-Helmholtz equation $\Delta_r G = \Delta_r H - T \times \Delta_r S$ the following equation is obtained:

$$\ln K = - \frac{\Delta_r H^0}{R} \times \frac{1}{T} + \frac{\Delta_r S^0}{R}. \quad (18)$$

We assume that the temperature dependence of $\Delta_r H^0$ and $\Delta_r S^0$ is small and can therefore be neglected. Equation (18) was then fitted as linear equation $\ln K_h$ vs. $1/T$, where $- \frac{\Delta_h H^0}{R}$ denotes the slope and $\frac{\Delta_h S^0}{R}$ the intercept of the resulting curve (**Figure 14**). A linear relationship is indeed found, and despite the small data basis the experimental uncertainty is relatively small. The obtained values for $\Delta_h H^0$ and $\Delta_h S^0$ presented in **Table 5** are in good agreement with literature data. A closer look on the highly negative enthalpy of hydration ($\Delta_h H^0$ = –238 kJ·mol^{-1}) explains why the dehydration only occurs at low $p(H_2O)$ and high temperature, i.e. mayenite is strongly hygroscopic. For the sake of completeness, we present the equilibrium constant as function of temperature:

$$\ln K_h = 2.87 \times 10^4 \frac{\mathrm{K}}{T} - 14.2. \quad (19)$$

Hydration of ceramic materials has been underestimated for a long time, and studies were restricted to the field of proton-conducting ceramics for intermediate temperature SOFC. Recently, more studies from the background of possible effects on the ionic conductivity were performed.[16, 45] In most cases and in contrast to O-mayenite (see Section 2), proton conduction was held responsible for the change in conductivity upon variation in humidity, especially at lower temperatures. The hydration of perovskite-based materials turned out to be a real bulk process with chemical diffusion of H_2O into the entire volume.[58-61] In fluorite-type oxides (Zirconia, Ceria) hydration appears to be more a surface/interface process inside grain boundaries.[62, 63] Kim *et al.* did not observe any significant effect on the conductivity of nano-crystalline ceria in hydration experiments.[64] Recently, Gregori *et al.* investigated the conductivity of dense and porous nanocrystalline ceria thin films at temperatures below 500 °C under wet and dry conditions.[65] They only observed a conductivity increase for the porous material under wet conditions. Pietrowski *et al.* monitored the water desorption kinetics in nano-YSZ and single crystalline YSZ at room temperature by IR-spectroscopy and observed a much slower loss of water for the nanocrystalline sample.[66] Both authors draw the conclusion that water must be adsorbed on the internal surface (pores, cracks, channels) of the materials due to the open porosity. Concerning O-mayenite, hydration is a bulk-related diffusion and reaction process, since in case of a surface/interface process the observed course of $\lg\sigma$ vs. $\lg p\mathrm{H_2O}$ cannot be explained.

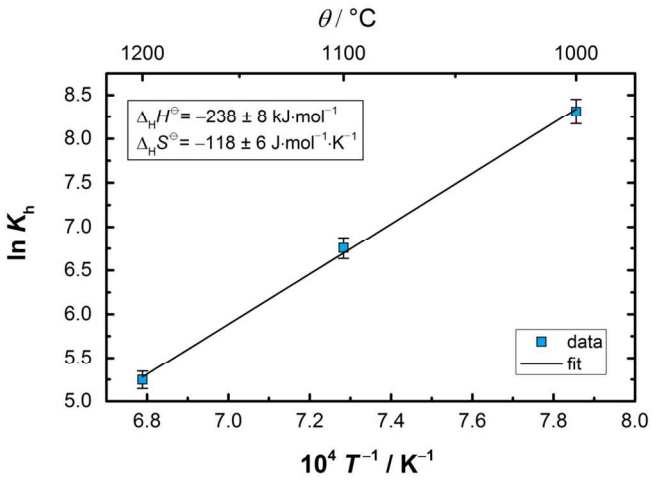

Figure 14. Van't Hoff plot for hydration of O-mayenite. *K* values were experimentally obtained by conductivity measurements and defect-chemical calculations.

Table 5. Thermodynamic parameters for the hydration of O-mayenite obtained by fitting of experimental data.

	this work	**Hayashi *et al.*[15]**	**Strandbakke *et al.*[16]**
$\Delta_h H^0$ / kJ×mol^{-1}	−238 ± 8	−228 ± 20	−240 ± 16
$\Delta_h S^0$ / J×mol^{-1}×K^{-1}	−118 ± 6	−117 ± 10	−123 ± 10

In summary, the conductivity of O-mayenite was explored in a wide range of water vapour partial pressure. The resulting data were modelled within an equilibrium defect-chemical approach, and the degree of hydration and the corresponding thermodynamic parameters are obtained. In agreement with previous studies we could verify that the hydration of mayenite is a bulk transport process rather than a surface/interface reaction.

5. Conclusion

We successfully prepared pure and anion substituted mayenite $C_{12}A_7$:X with a variety of cage anions (X = O, Cl, F, CN, S, N). The phase purity of the obtained samples was affirmed with XRD and Raman spectroscopy. Electrical conductivity was measured with impedance spectroscopy and turns out to be considerably lower for substituted mayenite than for O-mayenite accompanied by much higher activation energy. Only cage oxygen ions in mayenite are able to diffuse via the energetically favoured interstitialcy mechanism. A partial replacement re-oxidation of substituted materials, i.e. a replacement of substituted cage anions by oxygen at high temperatures cannot be excluded, but implies a certain mobility of the foreign cage anion species. The measured anion conductivities are probably too low for applications at low temperatures in comparison to other common oxygen ion conductors (e.g. YSZ, CGO, BICUVOX, LSM), and values higher than 1µS/cm were only observed for temperature above 700 °C. At temperatures of about 900 °C the conductivities approach values up to 1 mS/cm.

In order to resolve uncertainties in the literature about the stability of O-mayenite under different thermodynamic conditions, a degradation study was also performed. It clearly turned out that mayenite is not stable under dry conditions ($p(H_2O) \approx 10^{-5}$ bar) at temperatures above 1050 °C. At lower temperatures mayenite is kinetically stabilized due to limited Ca diffusivity. Hydroxyl ions inside the cages appear to have a significant effect on the stability of mayenite, and the stability limit was found to be approx. 100 ppm H_2O (minimum value) in the surrounding gas atmosphere. Calcia-alumina phase diagrams for the dry and wet state are presented, and it is shown that $C_{12}A_7$ vanishes from the phase diagram under dry conditions.

Finally, a closer look on the hydration process was taken from the perspective of defect chemistry. Only a few studies in the literature considered this general topic on other material systems, and even less measured the conductivity in such a wide range of water vapour partial pressure pH_2O as done in this work. The obtained hydration data were successfully fitted with a point defect model and the thermodynamic parameters of the hydration reaction were evaluated. They are in good agreement literature data, and we consider our model as reasonable.

We conclude that the approach to use mayenite as a crystalline solvent for various anions works well from the thermodynamic and structural perspective: In fact, we were successful to substitute cage oxygen by various foreign anions. However, the resulting electrolytes show much lower conductivities than O-mayenite, and re-oxidation takes place at elevated temperature in oxygen-containing atmospheres. Therefore, they are unfortunately not suited as high temperature electrolytes for applications. Moreover, there are up to today no suitable high temperature electrolytes for other anions than oxygen and fluorine with the potential for application. We also conclude that hydration/dehydration of mayenite can easily cause problems, as the $p(H_2O)$ controls the stability of the O-mayenite phase itself. The sensitivity toward H_2O has already quite early been recognized by Irvine and West[28], but a better understanding of the underlying reactions has only been achieved more recently, including the present study.

AUTHOR INFORMATION

Corresponding Author

*Juergen.janek@phys.chemie.uni-giessen.de

Author Contributions

The manuscript was written through contributions of all authors. All authors have given approval to the final version of the manuscript.

Funding Sources

This work was supported by the German Research Foundation (DFG) within the joint project PAK 596 (DFG Ja648/20-1 and DFG Le781/14-1).

ACKNOWLEDGMENT

Stefan G. Ebbinghaus and Holger Krause (Martin-Luther-Universität Halle-Wittenberg, Halle/Saale, Germany) are gratefully acknowledged for providing polycrystalline and single crystalline O-mayenite samples. The authors acknowledge support by the Laboratory for Materials Research (LaMa) at JLU Giessen.

1 G. I. Zhmoidin and A. K. Chatterjee, *Cem. Concr. Res.*, 1984, **14**, 386-396.
2 R. N. Edmonds and A. J. Majumdar, *Cem. Concr. Res.*, 1988, **18**, 473-478.
3 D. E. Macphee and E. E. Lachowski, in *Lea's Chemistry of Cement and Concrete*, ed. P. C. Hewlett, Elsevier, 4th edn., 2006, p. 111.
4 J. T. S. Irvine, M. Lacerda and A. R. West, *Mater. Res. Bull.*, 1988, **23**, 1033-1038.
5 M. Lacerda, J. T. S. Irvine, F. P. Glasser and A. R. West, *NATURE*, 1988, **322**, 525-526.
6 J. Jeevaratnam, F. P. Glasser and L. S. D. Glasser, *J. Am. Ceram. Soc.*, 1964, **47**, 105-106.
7 A. Schmidt, M. Lerch, J.-P. Eufinger, J. Janek, I. Tranca, M. M. Islam, T. Bredow, R. Dolle, H.-D. Wiemhöfer, H. Boysen and M. Hölzel, *Solid State Ionics*, 2014, **254**, 48-58.
8 J. Q. Sun, C. F. Song, S. Ning, S. B. Lin and Q. X. Li, *Chin. J. Chem. Phys.*, 2009, **22**, 417-422.
9 K. Hayashi, H. Muramatsu, S. Matsuishi, T. Kamiya and H. Hosono, *Electrochem. Solid-State Lett.*, 2009, **12**, J11.
10 H. Hosono and Y. Abe, *Inorg. Chem.*, 1987, **26**, 1192-1195.

11 H. Hosono, K. Hayashi, K. Kajihara, P. V. Sushko and A. L. Shluger, *Solid State Ionics*, 2009, **180**, 550-555.
12 Q. X. Li, K. Hayashi, M. Nishioka, H. Kashiwagi, M. Hirano, Y. Torimoto, H. Hosono and M. Sadakata, *Appl. Phys. Lett.*, 2002, **80**, 4259.
13 Y. Dong, H. Hosono and K. Hayashi, *RSC Adv.*, 2013, **3**, 18311-18316.
14 V. K. Singh and F. P. Glasser, *Ceram. Int.*, 1988, **14**, 59-62.
15 K. Hayashi, M. Hirano and H. Hosono, *J. Phys. Chem. B*, 2005, **109**, 11900-11906.
16 R. Strandbakke, C. Kongshaug, R. Haugsrud and T. Norby, *J. Phys. Chem. C*, 2009, **113**, 8938-8944.
17 A. Schmidt, M. Lerch, J.-P. Eufinger, J. Janek, R. Dolle, H.-D. Wiemhöfer, I. Tranca, M. M. Islam, T. Bredow, H. Boysen and M. Hoelzel, *Solid State Sci.*, 2014, **38**, 69-78.
18 S. Kim, M. Miyakawa, K. Hayashi, T. Sakai, M. Hirano and H. Hosono, *J. Am. Chem. Soc.*, 2005, **127**, 1370-1371.
19 H. Boysen, I. Kaiser-Bischoff and M. Lerch, *Diffusion Fundamentals*, 2008, **8**, 2.1-2.7.
20 J. M. Polfus, K. Toyoura, C. H. Hervoches, M. F. Sunding, I. Tanaka and R. Haugsrud, *J. Mater. Chem.*, 2012, **22**, 15828.
21 A. Schmidt, H. Boysen, A. Senyshyn and M. Lerch, *Z. Kristallogr.*, 2014, **229**, 427.
22 K. Hayashi, S. Matsuishi, T. Kamiya, M. Hirano and H. Hosono, *NATURE*, 2002, **419**, 462-465.
23 S. Matsuishi, K. Hayashi, M. Hirano and H. Hosono, *J. Am. Chem. Soc.*, 2005, **127**, 12454-12455.
24 K. Hayashi, *J. Solid State Chem.*, 2011, **184**, 1428-1432.
25 M. Lacerda, A. R. West and J. T. S. Irvine, *Solid State Ionics*, 1993, **59**, 257-262.
26 S. Matsuishi, Y. Toda, M. Miyakawa, K. Hayashi, T. Kamiya, M. Hirano, I. Tanaka and H. Hosono, *Science*, 2003, **301**, 626-629.
27 S. W. Kim, S. Matsuishi, T. Nomura, Y. Kubota, M. Takata, K. Hayashi, T. Kamiya, M. Hirano and H. Hosono, *Nano Lett.*, 2007, **7**, 1138-1143.
28 J. T. S. Irvine and A. R. West, *J. Appl. Electrochem.*, 1989, **19**, 410-412.
29 T. Kamiya, S. Aiba, M. Miyakawa, K. Nomura, S. Matsuishi, K. Hayashi, K. Ueda, M. Hirano and H. Hosono, *Chem. Mater.*, 2005, **17**, 6311-6316.
30 Y. Nishio, K. Nomura, H. Yanagi, T. Kamiya, M. Hirano and H. Hosono, *Mater. Sci. Eng. B*, 2010, **173**, 37-40.
31 H. Hosono, K. Hayashi, T. Kamiya, T. Atou and T. Susaki, *Sci. Technol. Adv. Mater.*, 2011, **12**, 034303.
32 S. Yang, J. N. Kondo, K. Hayashi, M. Hirano, K. Domen and H. Hosono, *Chem. Mater.*, 2003, **16**, 104-110.
33 F. Huang, J. Li, L. Wang, T. Dong, J. Tu, Y. Torimoto, M. Sadakata and Q. Li, *J. Phys. Chem. B*, 2005, **109**, 12032-12037.
34 J. Li, F. Huang, L. Wang, Z. Wang, S. Yu, Y. Torimoto, M. Sadakata and Q. Li, *J. Phys. Chem. B*, 2005, **109**, 14599-14603.
35 Y. Dong, K. Hayashi, H. Nozoe, Y. Shinoda and H. Hosono, *J. Am. Ceram. Soc.*, 2014, **97**, 4037-4044.
36 I. Kohatsu and G. W. Brindley, *Z. Phys. Chem.*, 1968, **60**, 79.
37 R. W. Nurse, J. H. Welch and A. J. Majumdar, *Trans. Br. Ceram. Soc*, 1965, **64**, 323.
38 R. W. Nurse, J. H. Welch and A. J. Majumdar, *Trans. Br. Ceram. Soc*, 1965, **64**, 409.
39 B. Hallstedt, *J. Am. Ceram. Soc.*, 1990, **73**, 15-23.

40 L. Palacios, Á. G. De La Torre, S. Bruque, J. L. García-Muñoz, S. García-Granda, D. Sheptyakov and M. A. G. Aranda, *Inorg. Chem.*, 2007, **46**, 4167-4176.
41 D. K. Lee, L. Kogel, S. G. Ebbinghaus, I. Valov, H. D. Wiemhoefer, M. Lerch and J. Janek, *Phys. Chem. Chem. Phys.*, 2009, **11**, 3105-3114.
42 H. Boysen, I. Kaiser-Bischoff, M. Lerch, S. Berendts, M. Hoelzel and A. Senyshyn, *Acta Phys. Pol. A*, 2010, **117**.
43 P. Sushko, A. Shluger, K. Hayashi, M. Hirano and H. Hosono, *Phys. Rev. B*, 2006, **73**, 014101.
44 K. Kajihara, S. Matsuishi, K. Hayashi, M. Hirano and H. Hosono, *J. Phys. Chem. C*, 2007, **111**, 14855-14861.
45 K. D. Kreuer, *Annu. Rev. Mater. Res.*, 2003, **33**, 333-359.
46 T. Norby, *MRS Bull.*, 2009, **34**, 923-928.
47 K. Hayashi, P. V. Sushko, A. L. Shluger, M. Hirano and H. Hosono, *J. Phys. Chem. B*, 2005, **109**, 23836-23842.
48 S. G. Ebbinghaus, H. Krause and F. Syrowatka, *Cryst. Growth Des.*, 2013, **13**, 2990-2994.
49 M. Lerch, J. Janek, K. D. Becker, S. Berendts, H. Boysen, T. Bredow, R. Dronskowski, S. G. Ebbinghaus, M. Kilo, M. W. Lumey, M. Martin, C. Reimann, E. Schweda, I. Valov and H. D. Wiemhöfer, *Prog. Solid State Chem.*, 2009, **37**, 81-131.
50 P. McMillan and B. Piriou, *J. Non-Cryst. Solids*, 1983, **55**, 221-242.
51 M. Ruszak, S. Witkowski, P. Pietrzyk, A. Kotarba and Z. Sojka, *Funct. Mat. Lett.*, 2011, **04**, 183-186.
52 M. Matsuda, Y. Inda, W. Hisamatsu, K. Yamashita and T. Umegaki, *J. Mater. Sci. Lett.*, 1996, **15**, 933-934.
53 M. G. H. M. Hendriks, J. E. ten Elshof, H. J. M. Bouwmeester and H. Verweij, *Solid State Ionics*, 2002, **146**, 211-217.
54 A. Pimenov, J. Ullrich, P. Lunkenheimer, A. Loidl and C. H. Rüscher, *Solid State Ionics*, 1998, **109**, 111-118.
55 J. H. Park and R. N. Blumenthal, *J. Electrochem. Soc.*, 1989, **136**, 2867-2876.
56 T. Otake, H. Yugami, K. Yashiro, Y. Nigara, T. Kawada and J. Mizusaki, *Solid State Ionics*, 2003, **161**, 181-186.
57 R. J. Panlener, R. N. Blumenthal and J. E. Garnier, *Journal of Physics and Chemistry of Solids*, 1975, **36**, 1213-1222.
58 D. K. Lim, B. Singh, S. Y. Jeon and S. J. Song, *J. Electrochem. Soc.*, 2013, **160**, F623-F628.
59 H. I. Yoo, J. Y. Yoon, J. S. Ha and C. E. Lee, *Phys. Chem. Chem. Phys.*, 2008, **10**, 974-982.
60 D. V. Korona, I. M. Kutikov and A. Y. Neiman, *Russ. J. Electrochem.*, 2013, **49**, 1171-1180.
61 J. H. Yu, J. S. Lee and J. Maier, *Angew. Chem. Int. Ed.*, 2007, **46**, 8992-8994.
62 S. Miyoshi, Y. Akao, N. Kuwata, J. Kawamura, Y. Oyama, T. Yagi and S. Yamaguchi, *Solid State Ionics*, 2012, **207**, 21-28.
63 W. C. Chueh, C. K. Yang, C. M. Garland, W. Lai and S. M. Haile, *Phys. Chem. Chem. Phys.*, 2011, **13**, 6442-6451.
64 S. Kim, R. Merkle and J. Maier, *Solid State Ionics*, 2003, **161**, 113-119.
65 G. Gregori, M. Shirpour and J. Maier, *Adv. Funct. Mater.*, 2013, **23**, 5861-5867.
66 M. J. Pietrowski, R. A. De Souza, S. Kim, Z. A. Munir and M. Martin, *Solid State Ionics*, 2012, **225**, 241-244.